



Comparative assessment of MEGAN v2.1 and v3.2 biogenic VOC emissions over the Qinghai-Tibet Plateau: implications for summertime surface ozone simulations

Ping LI^{1, 2}, Ye YU^{1, 2, 3}, Suping ZHAO^{1, 2, 3}

- ¹State Key Laboratory of Cryospheric Science and Frozen Soil Engineering, Northwest Institute of Eco-Environment and Resources, Chinese Academy of Sciences, Lanzhou 730000, Gansu, China;
 ²University of Chinese Academy of Sciences, Beijing 100049, China;
 ³Pingliang Land Surface Process and Severe Weather Research Station, Pingliang 744015, Gansu, China
 *Correspondence: Ye YU (yyu@lzb.ac.cn)
- 10 Abstract. Biogenic volatile organic compounds (BVOCs) constitute a significant precursor to tropospheric ozone (O₃) over the Qinghai-Tibet Plateau (QTP), yet substantial uncertainties persist in BVOC emission inventories for this high-altitude region. This study employs the WRF/CMAQ model to systematically compare BVOC emissions between MEGAN v2.1 and v3.2 over the QTP, and their impacts on surface O₃ simulations for August 2022. MEGAN v3.2 yields total BVOC emissions (127.96 Gg) 44% lower than v2.1 (229.67 Gg), with isoprene emissions 1.7 times lower and monoterpenes 0.3 times higher. Spatially, the most pronounced differences occur in southeastern Tibet and the Hengduan Mountains. Indirect constraints using TROPOMI formaldehyde (HCHO) vertical column densities (VCDs) and OMI/MLS total-column ozone (TCO) reveal that CMAQ simulations with v3.2 BVOC emissions exhibit a marginally stronger correlation with satellite HCHO VCDs (r = 0.34 vs 0.32, p < 0.01), while the simulated TCO agree similarly with the OMI/MLS TCO. Simulations with both inventories indicate that incorporating BVOCs increase regional average MDA8 O3 concentrations by 2-3%. However, in Lhasa, Xining, and certain cities within the Hengduan Mountains, increases reach 5-14%. In southeastern Tibet, where NO_x is extremely scarce, the response is negligible. Due to its elevated isoprene emissions, MEGAN v2.1 increases the MDA8 O3 concentrations by up to 19.61% in the aforementioned cities-nearly twice those in v3.2. It is recommended that v3.2 be prioritized for air quality modelling in pristine alpine region. These findings provide valuable guidance for designing effective air quality management policies over the QTP.





1 Introduction

45

50

55

Biogenic Volatile Organic Compounds (BVOCs) from terrestrial vegetation play a crucial role in atmospheric chemistry (Atkinson and Arey, 2003; Guenther et al., 2006). They react with hydroxyl radical (OH), nitrate radical (NO₃), and ozone (O₃), and serve as important precursors for tropospheric O₃ (Gu et al., 2021). Cao et al. (2022) estimated that the summertime BVOC emissions led to an average increase of 8.6 ppb (17%) in daily maximum 8 h (MDA8) O₃ concentration over China in summer 2018. As a key input for chemical transport models (CTMs), accurately quantifying BVOC emissions is essential for improving CTMs performances, which in turn will support the development of effective air pollution control strategies (Borge et al., 2014). BVOCs, primarily composed of isoprenoids (such as isoprene and monoterpenes), alcohols, carbonyls and acids, are biosynthesized and emitted by plants as adaptive responses to environmental changes (Šimpraga et al., 2019), herbivory (Yu et al., 2021) or to attract pollinators (Pichersky and Gershenzon, 2002). BVOC emissions are influenced by a range of abiotic and biotic factors, among which temperature and solar radiation are considered the most critical (Loreto and Schnitzler, 2010; Feldner et al., 2022; Lun et al., 2020; Peron et al., 2021; Possell and Loreto, 2013). Due to limited understanding of the underlying biochemical mechanisms, current BVOC emission models predominantly adopt an empirical bottom-up approach, where emission factors are defined as functions of environmental variables. One of the most widely used BVOC emission models is MEGAN (Model of Emissions of Gases and Aerosols from Nature), developed by Guenther et al. (2006, 2012, 2020). MEGAN v2.1, released in 2012, employs a method to estimate BVOC emissions based on plant function type (PFT)-specific emission factors and PFT distributions data. However, studies have shown that different plant species emit distinct BVOCs blends and display divergent temperature responses (Grote et al., 2013). This interspecific variability introduces substantial uncertainties in BVOC emission estimates derived from PFT-based emission factors. Notably, Ciccioli et al. (2023) argued that the PFT-based approach may insufficiently resolve species-level emission characteristics, especially in ecosystems with high biodiversity. The latest MEGAN version 3.2 (MEGAN v3.2) incorporates species-specific emission factors and utilizes global ecoregion data based on plant species composition, in order to improve the accuracy of BVOC emission estimates (Guenther et al., 2020). Although, MEGAN model has been widely used to investigate the impacts of BVOC emissions on atmospheric chemistry in China (Gao et al., 2022; Lou et al., 2023; Ma





et al., 2019; Wang et al., 2023b), comparative evaluations of the performance of MEGAN versions 2.1 and 3.2 remain limited.

The Qinghai-Tibet Plateau (QTP), known as "the Third Pole" and "the Roof of the World", has an extremely low population density compared to other regions, resulting in minimal human activities and limited anthropogenic disturbances to the natural ecosystem. These characteristics make it one of the cleanest regions in the world (Huang et al., 2023). However, recent studies have documented a continuous increase in surface O3 concentrations across the QTP, posing a growing threat to the local ecosystem and human health (Chen et al., 2022). According to Ye et al. (2024), surface O₃ over the QTP is predominantly influenced by regional background processes, namely stratospheric ozone intrusion (contributing at least 25%) and long-range transport from South Asia (9.45%-20.28%); in contrast local photochemical production plays a relatively minor role (5.24%-10.46%) (Yin et al., 2023). More recently, Xu et al. (2024) reported that surface O₃ over the QTP exhibited a faster increase at urban stations (1.71 ppb yr⁻¹) compared with background stations (0.26 ppb yr⁻¹), which they attributed to enhanced non-local transport and local emissions. The QTP covers an area of approximately 2.57 million km², with more than 60% of its surface occupied by vegetation (Chen et al., 2020), and hosts over 12,000 species of seed plants (Zhang et al., 2016). Nevertheless, BVOC emissions in this region remain poorly quantified. Considering the relatively minor contribution of anthropogenic sources, BVOCs are likely to play an important role in driving local O₃ photochemical production over the QTP. Under the context of climate change and land-cover dynamics in this region, it is essential to improve our understanding of BVOC emissions and their influence on O₃ formation over the QTP.

This study aims to systematically evaluates the BVOC emissions estimated by two different versions of the MEGAN (v2.1 and v3.2) and assesses their impacts on O₃ simulations over the QTP using WRF-CMAQ modeling results. Numerical experiments were conducted for August 2022 to capture the period of peak photosynthetic and biological activity. This study provides new insights into the role of BVOCs in controlling O₃ formation within this high-altitude and ecologically vulnerable region.





2 Materials and Methods.

2.1 Study area

90

The Qinghai-Tibet Plateau (QTP) (26-39°N, 73-104°E) is located in the southwestern part of China, encompassing Qinghai, Tibet and parts of Xinjiang, Sichuan and Yunnan provinces (Fig. 1). The average annual temperature in QTP varies from -15°C to 10°C (You et al., 2013). Precipitation follows a distinct spatial gradient, decreasing from over 1,000 mm in the humid southeast to less than 100 mm in the arid northwest (Kuang and Jiao, 2016). Corresponding to this climatic gradient, the vegetation distribution across QTP displays a distinct zonal pattern: broadleaf forests are dominate in the humid southeastern regions, alpine meadows prevail across the central areas, and alpine steppes characterize the arid northwestern zones (Han et al., 2023). The growing season for most vegetation on the QTP typically spans from April to October, culminating in peak photosynthetic and biological activity during July and August (Sun et al., 2020; Che et al., 2014).

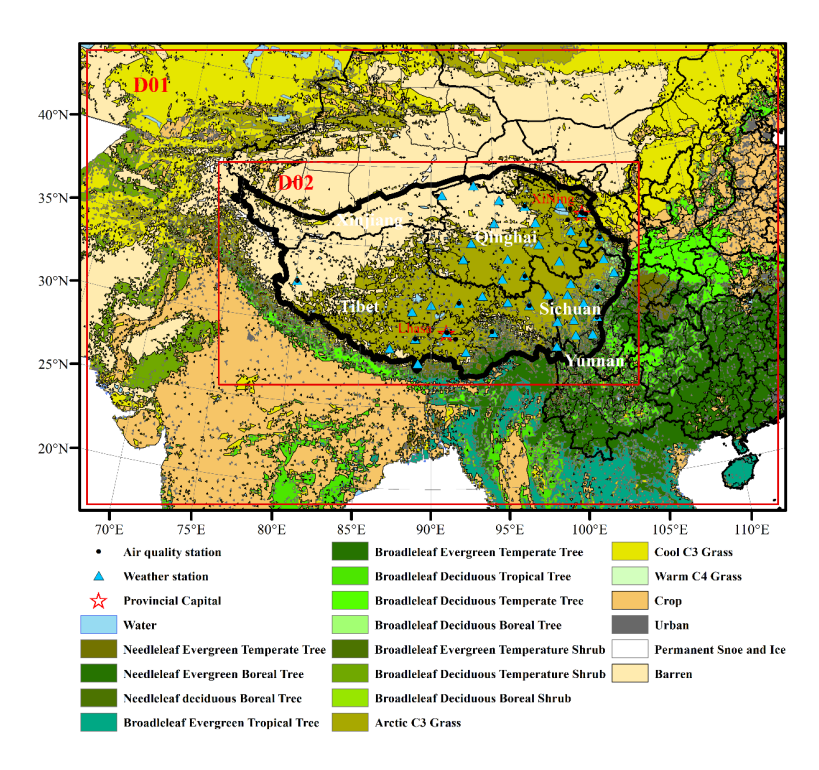


Figure 1: Map of the study area. Model domains (red boxes), plant function types (PFTs, coloured areas), and the locations of meteorological stations (blue triangles) and air quality monitoring stations (black dots).





2.2 Ground observation data

2.2.1 Meteorological data

Meteorological variables, including 2 m temperature (T2), 10 m wind speed (WS10), and 10 m wind direction (WD10), were acquired from 25 meteorological stations across the QTP (see blue triangles in Fig.1) via the National Climate Data Center (NCDC). WS10 and WD10 were used to derive the zonal (u10) and meridional (v10) wind components. These data, recorded at 3-hour intervals, were used to evaluate the simulated meteorological fields in this study.

105 2.2.2 Surface O₃ Concentrations

Hourly surface ozone concentrations were obtained from the China National Environmental Monitoring Center. Data quality assurance and control procedures followed the technical guidelines outlined in the National Environmental Protection Standards of the People's Republic of China (HJ 630-2011). Stations with valid data less than 75% in August 2022 were excluded. After quality control, 30 stations were selected, with their locations shown in Fig. 1 as black dots.

2.3 Satellite Remote Sensing data

110

115

120

2.3.1 Vegetation-specific leaf area index (LAIv)

The MEGAN quantifies foliage abundance in a landscape using the vegetation-specific leaf area index (LAIv), defined as the leaf area index (LAI) per vegetated cover fraction (VCF). In this study, LAIv was derived using the MODIS MOD15A2H V6.1 and MOD44B.006 datasets for the period of August 2022.

2.3.2 Plant Functional Type (PFT)

The MODIS MCD12Q1.061 LC_Type5 classifications for the year 2022 was directly utilized to identify the seven PFTs, i.e. needleleaf evergreen trees, needleleaf deciduous trees, broadleaf evergreen trees, broadleaf deciduous trees, shrubs, grass, and crop. The global monthly climatologies of surface air temperature and precipitation from WorldClim were used to reclassify the 7 PFTs into 15 PFTs. The reclassification was conducted following the climate-based rules outlined in Bonan et al. (2002). As

125

130

135

140

145





illustrated in Fig. 1, the land cover over the QTP exhibits a clear gradient, transitioning progressively from forest-dominated regions in the southeast, through grassland-centred central regions, to largely barren land in the northwest. The dominant PFTs across the QTP include Arctic C3 grass, needleleaf evergreen boreal tree, needleleaf evergreen temperature tree, broadleaf evergreen temperature tree, broadleaf deciduous boreal tree, and broadleaf deciduous temperature tree.

2.3.3 Formaldehyde (HCHO) vertical column density (VCD)

The emissions of BVOCs, particularly isoprene and terpenes, serves as a significant source of precursors for HCHO (Trimmel et al., 2023). Accordingly, HCHO has been used in previous studies as an indirect indicator for evaluating BVOC simulations (Wang et al., 2021a). The Sentinel-5P TROPOMI daily offline level 3 (OFFL L3) HCHO dataset, with a spatial resolution of 1113.2 m × 1113.2 m and covering the period from August 1 to 31, 2022, obtained from the Google Earth Engine cloud platform, was used to assess the estimated BVOC emissions. To minimize anomalies, we excluded data with cloud fraction greater than 0.3, solar zenith angle exceeding 70°, and vertical column density values outside the range of -0.8×1015 and 7.6×1015 molec cm⁻² (Zhu et al., 2017).

2.3.4 Tropospheric Column Ozone (TCO)

The OMI/MLS monthly-mean TCO dataset, with a spatial resolution of $1^{\circ} \times 1^{\circ}$, was used to evaluate the simulated TCO concentrations. TCO was derived from the OMI and MLS instruments on board the Aura satellite and calculated using the tropospheric ozone residual (TOR) method, which involves subtracting the MLS stratospheric column ozone from the OMI total column ozone after adjusting for calibration differences between the two instruments (Ziemke et al., 2006, 2011).

2.4 Model descriptions and Experimental Design

2.4.1 MEGAN model for BVOC Emissions

MEGAN is a widely used modeling framework for estimating fluxes of biogenic compounds between terrestrial ecosystems and the atmosphere. It employs simplified mechanistic algorithms to represent the primary known processes that regulate emissions from biogenic sources. The biogenic emission (F_i) (μg)

160

165

170

175





 $m^{-2}\,h^{-1}$) of a given compound (i) is estimated based on the weighted average of the emission factors (EF_i) ($\mu g \ m^{-2} \ h^{-1}$), and activity factor (γ_i), which are influenced by environmental conditions:

$$F_i = EF_i \times \gamma_i \tag{1}$$

The MEGAN v2.1 and MEGAN v3.2 implement different approaches for calculating EF_i. In MEGAN v2.1, EF_i is determined based on PFT-specific emission factor $(\epsilon_{i,j})$ and the area coverage fraction $(f_{PFT(j)})$ of each PFT (j) in a grid box:

$$EF_i = \sum \varepsilon_{i,j} f_{PFT(j)}$$
 (2)

In contrast, MEGAN v3.2 calculates EF_i using plant species-specific emission factor $(\varepsilon_{i,k})$ and the area coverage fraction $(f_{Species(k)})$ of each plant species (k) in a grid box:

$$EF_i = \sum \varepsilon_{i,k} f_{\text{Species}(k)}$$
 (3)

For MEGAN v2.1, the PFTs data as detailed in Section 2.3.2 were used. For MEGAN v3.2, the default ecotype and growth data provided within the model were employed. During the following simulations, only the default functions in MEGAN were applied to ensure consistency with the standard model configuration.

2.4.2 WRF/CMAQ Model Configuration

In this study, the US EPA's CMAQ version 5.4 was used with a modified version of the Carbon-Bond Mechanism version 6 (CB6R3) chemical mechanism. Fig. 1 shows the CMAQ modelling domain (the red boxes) that consists of two nested domains with spatial resolutions of 27 and 9 km. Vertically there are 44 σ -layers extending from the surface to an altitude of 50 hPa. The default ICON/BCON program was employed to generate the initial and boundary conditions for the CMAQ 27 km simulation, while the initial and boundary conditions for the 9 km simulation were derived from the results of the 27 km simulation.

The WRF-ARW version 4.4.2 was used to generate the hourly meteorological fields for MEGAN, SMOKE, and CMAQ. The WRF was configured to have two nested domains, covering and aligning with the CMAQ domains with each of the WRF domain being at least four grid cells larger than the corresponding CMAQ domains. The Final (FNL) Operational Global Analysis data of the National Centers for Environmental Prediction (NCEP), with a spatial resolution of 1°×1° and updated every 6 hours, were used as the initial and boundary conditions for WRF simulations. The simulations began at 00:00 UTC on July 27, 2022 and ended at 23:00 UTC on August 31, 2022. The first five simulation days

185

190





were used as "spin-up" period to minimize the influence of initial conditions. The key physical and chemical parameterizations used in the WRF-CMAQ simulations are listed in Table 1.

Anthropogenic emissions within China were obtained from the 2020 Multi-resolution Emissions Inventory (MEIC2020) and processed using the MEIAT-CMAQ (Wang et al., 2024b). For regions outside China, anthropogenic emissions were sourced from the 2018 Emissions Database for Global Atmospheric Research (EDGAR v6.1) and processed using SMOKE v4.7. Biomass burning emissions were derived from the Fire Inventory from NCAR version 2.5 (FINN v2.5) (Wiedinmyer et al., 2023) and integrated using FINN2CMAQ.

To investigate the differences in the estimated BVOCs by the two versions of MEGANs and their impact on O_3 concentrations, three experiments with different BVOC emission schemes were conducted (see Table 2). The BVOC emissions estimated using MEGAN v2.1 and MEGAN v3.2 were compared and their correlations with observed HCHO VCD was analyzed. The impact of BVOC emissions on O_3 simulations was evaluated by examining the differences between simulations with and without BVOC emissions.

Table 1 Physical and chemical options in the WRF/CMAQ simulation.

	Process	Option				
	Microphysics	WRF Single-Moment 6-class (Hong and Lim, 2006)				
Physical	Surface Layer	Yonsei University Scheme (Hong et al., 2006)				
	Shortwave/Longwave	NCAR Community Atmospheric Model (Collins et al.,				
	radiation	2004)				
	Land surface model	Noah land surface model (Chen et al., 1996; Chen and				
		Dudhia, 2001)				
	Cumulus Parameterization	Kain-Fritsch (Kain, 2004)				
	Photolysis scheme	In-line Photolysis (Binkowski et al., 2007)				
Chemical	Gas-phase chemistry	CB6R3 (Emery et al., 2015)				
	Aerosol module	AERO7 (Appel et al., 2021)				

Table 2 Numerical experiments

Experiments	Emissions
NoBVOC	Anthropogenic emissions + Biomass burning
InBVOCv2.1	Anthropogenic emissions + Biomass burning + MEGAN v2.1
InBVOCv3.2	Anthropogenic emissions + Biomass burning + MEGAN v3.2

https://doi.org/10.5194/egusphere-2025-5579 Preprint. Discussion started: 19 November 2025

© Author(s) 2025. CC BY 4.0 License.

195

200

205

210





2.5 Determination of O₃ production sensitivity regimes

Photochemical indicators, such as VOC/NO_x, HCHO/NO₂, H_2O_2/HNO_3 , and O_3/HNO_3 , are widely used to diagnose O_3 production regimes as they can be derived directly from observations or chemical transport models (Sillman and He, 2002; Li et al., 2022; Jin and Holloway, 2015). In this study, we apply the tropospheric HCHO/NO₂ ratio as the diagnostic metric. Vertical column densities of tropospheric HCHO and NO_2 between 15:00 and 18:00 local time for August 2022 were obtained from CMAQ simulations used to calculate the HCHO/NO₂ ratio; the threshold value that marks the transition between NO_x -limited and VOC-limited regimes was assumed to occur at HCHO/NO₂ = 2.5-4.5 following Ren et al. (2022).

3 Results and Discussions

3.1 Model Performance Evaluation

3.1.1 Meteorological Field Simulation (WRF)

To evaluate the model performance, statistical metrics including correlation coefficients (r), mean bias (MB), root-mean-square error (RMSE) and the Index of Agreement (IOA) were calculated. Table 3 summarizes the statistical results of the WRF-simulated hourly T2, u10 and v10 for the 25 meteorological stations, and the corresponding scatter plots are shown in Fig. S1. The performance of WRF in simulating T2 was good, with IOA and r of 0.88 and 0.82, respectively. The model slightly underestimated T2, with MB and RMSE of -1.93 and 4.00°C, respectively. In contrast, the model's performance in capturing wind speed was relatively poor, with IOA for u10 and v10 being 0.58 and 0.55, respectively, and the corresponding r being 0.30 and 0.27, respectively. The model modestly underestimated the u10 and overestimated the v10. The complex topography of the QTP poses significant challenges for simulating wind fields compared to other meteorological fields (Lu et al., 2022). Nevertheless, our results align closely with those reported in previous studies (Yang et al., 2020; Hu et al., 2024). These results demonstrate that the WRF model successfully reproduced meteorological conditions over the study region and can thus provide reliable meteorological inputs for MEGAN, SMOKE and CMAQ.

215

235

240





Table 3 Performance statistics for simulated meteorological variables.

	Obs mean	Sim mean	MB	RMSE	IOA	r
T2 (°C)	16.06 ± 5.79	14.07 ± 5.74	-1.93	4.00	0.88	0.82
u10 (m s ⁻¹)	$\textbf{-0.38} \pm 2.10$	-0.91 ± 2.50	-0.50	2.79	0.58	0.30
v10 (m s ⁻¹)	0.33 ± 1.84	0.58 ± 2.17	0.25	2.45	0.55	0.27

3.1.2 Surface O₃ Simulation (CMAQ)

Table 4 summarizes the performance statistics of the CMAQ-simulated surface MDA8 O₃ concentrations for the 30 air quality stations, and the corresponding scatter plots are shown in Fig. S2. The model consistently overestimated O₃ levels across all simulations. The highest MB occurred in experiment InBVOCv2.1, while the lowest MB was observed in experiment NoBVOC. A similar pattern was found for the RMSE. All experiments exhibited correlation coefficients (r) values exceeding 0.3 and IOA values exceeding 0.4, which is consistent with previous modeling studies over complex terrain (Hu et al., 2024).

Table 4 Performance statistics for simulated MDA8 O₃ concentrations in August 2022.

Experiments	Obs mean	Sim mean	MB	RMS	IOA	r
	$(\mu g m^{-3})$	$(\mu g m^{-3})$		E		
NoBVOC		133.60 ± 30.43	30.89	43.87	0.46	0.33
InBVOCv2.1	102.71 ± 21.93	141.75 ± 35.09	39.04	51.10	0.45	0.41
InBVOCv3.2	_	138.73 ± 31.66	36.03	47.84	0.44	0.35

3.2 BVOC emissions: MEGAN v2.1 vs. MEGAN v3.2

The total BVOC emissions simulated by MEGAN v2.1 over the QTP for August 2022 are 229.67 Gg, of which isoprene and monoterpene accounted for 56.49% (129.73 Gg) and 11.82% (27.14 Gg), respectively. In comparison, MEGAN v3.2 estimated a lower total emissions of 127.96 Gg, with isoprene and monoterpene contributing 37.68% (48.22 Gg) and 27.96% (35.78 Gg), respectively. On average, the isoprene emissions simulated by MEGAN v2.1 were 1.7 times higher than those of MEGAN v3.2, while monoterpene emissions were approximately 0.3 times lower. On the QTP, the forests emitted the most BVOCs, with an average contribution of 70.25% for MEGAN v2.1 and 74.85% for MEGAN v3.2, followed by the grasslands (20.45% for MEGAN v2.1 and 16.48% for MEGAN v3.2), and the other land use types only contributed 9.31% for MEGAN v2.1 and 8.67% for MEGAN v3.2. Overall, the BVOC

245

250

255

260

265

270





emissions accounted for $58.33 \pm 44.16\%$ and $56.23 \pm 41.58\%$ of the total VOCs (TVOCs) (TVOCs = BVOCs + AVOCs + Biomass burning VOCs) emissions for MEGAN v2.1 and MEGAN v3.2 in August over the QTP, respectively. The values even reached 100% in remote and suburban areas.

The BVOC emissions estimated in this study for Qinghai province are markedly lower than the top-down estimate of Li et al. (2023) and the G95-based estimate of Wang et al. (2023a) using locally measured emissions factors (Table S1). Nevertheless, the range of estimated annual total BVOC emissions for this region is wide: 10.70-455.60 Gg C for Qinghai and 187.00-577.80 Gg C for Tibet (Klinger et al., 2002;

Yin et al., 2020). Our estimates lie within these bounds. The discrepancies in BVOCs emission estimates among different studies can be attributed to variations in simulation periods, model algorithms, emission factors, land cover datasets, and meteorological conditions.

Figure 2 illustrates the spatial distribution of isoprene and monoterpene emission rates simulated by MEGAN v2.1 and MEGAN v3.2. Although the spatial patterns are similar, the magnitudes differ. The monthly average isoprene emission rate simulated by MEGAN v2.1 ranged from 0 to 0.48 ton grid⁻¹ h⁻¹ (mean: 0.006 ± 0.028 ton grid⁻¹ h⁻¹), while MEGAN v3.2 produced a lower range of 0 to 0.20 ton grid⁻¹ h⁻¹ (mean: 0.002 ± 0.011 ton grid⁻¹ h⁻¹). The monthly average monoterpene emission rate simulated by MEGAN v2.1 ranged from 0 to 0.08 ton grid⁻¹ h⁻¹ (mean: 0.001 ± 0.005 ton grid⁻¹ h⁻¹). In contrast, MEGAN v3.2 produced higher values, ranging from 0 to 0.13 ton grid⁻¹ h⁻¹ (mean: 0.002 ± 0.008). The differences between the two MEGAN versions were most pronounced in southeastern Tibet and the Hengduan Mountains region, areas characterized by high forest density (Fig. 1) and biodiversity (Li et al., 2020; López-Pujol et al., 2006).

Discrepancies in BVOC emissions between the two MEGAN versions stem from different approaches for assigning emission factors (EFs) (Eq. (2) vs Eq. (3)) and differences in the underlying emission processes, such as temperature and light responses, represented in each model (Guenther et al., 2020). In addition, MEGAN v3.2 includes an updated species-specific emission factor (ε) database, resulting in differences in EFs between the two versions. The isoprene EF from MEGAN v3.2 was lower than that from MEGAN v2.1 (Fig. S3). In contrast, the monoterpene EF was lower in southeastern Tibet and the Hengduan Mountains region, but higher across most other regions. MEGAN v3.2 also incorporated previously unrepresented BVOC emission processes, such as canopy heterogeneity, which can alter activity factors. Overall, the activity factors for isoprene and monoterpenes differed only slightly between

285





the two versions across most regions, but showed pronounced differences in southeastern Tibet and northwest QTP, where MEGAN v3.2 have substantially higher and lower values, respectively (Fig. S4). Guenther et al. (2020) reported that MEGAN v3 yields lower isoprene emissions than MEGAN v2.1, which is consistent with our findings. However, their study indicated that MEGAN v3 also produces lower monoterpene emissions than MEGAN v2.1. This is in contrast to our results: the higher monoterpene EFs over grasslands and the enhanced activity factors over southeastern Tibet in MEGAN v3.2 resulted in higher monoterpene emissions compared to MEGAN v2.1.

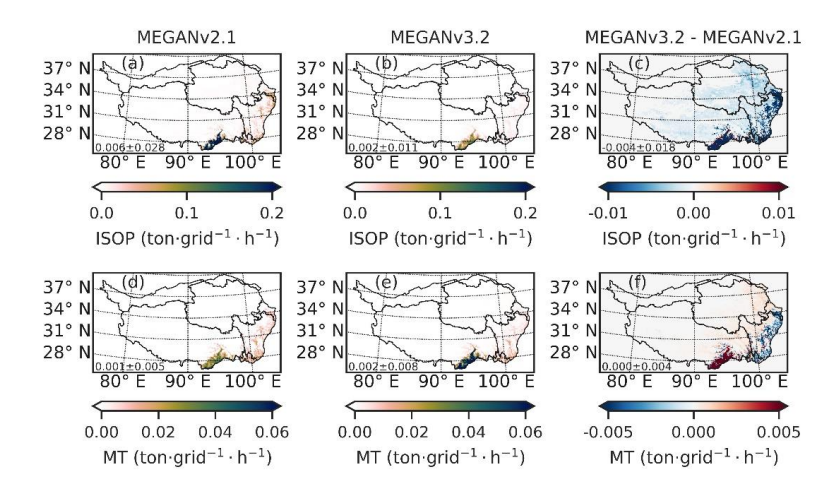


Figure 2: Spatial distribution of August average isoprene and monoterpene emission rate (ton grid h h) over the QTP simulated by MEGAN v2.1 (a, d) and MEGAN v3.2 (b, e) and their differences (c, f).

3.3 Evaluation of BVOC Emission Estimates Using Satellite Products

Due to the absence of in situ BVOC measurements over the QTP, direct evaluation of the two versions of MEGAN is unfeasible. This limitation necessitates the use of alternative proxy-based evaluation approaches. Formaldehyde (HCHO), an intermediate product in the oxidation of most VOCs, has been widely used as a tracer to constrain BVOC emissions in previous studies (Guion et al., 2023; Wang et al., 2022). In this study, satellite-derived HCHO vertical column densities (VCDs) are employed to assess the performance of both MEGAN versions. Additionally, tropospheric column ozone (TCO) is used as a

290

295

300

305

310

315





supplementary indicator, given its close linkage with photochemical processes driven by VOC oxidation processes.

3.3.1 Constraints from HCHO Vertical Column Densities

To evaluate the performance in estimating the spatial distributions of BVOC emissions by the two versions of MEGAN, the correlation between simulated HCHO vertical column densities (VCDs) by experiments InBVOCv2.1 and InBVOCv3.2 and satellite-derived HCHO VCDs, was firstly analysed (Fig. 3d). The spatial distribution of MEGAN v3.2 simulated HCHO VCDs in August exhibited a stronger correlation (r = 0.34, p < 0.01) with satellite-observed HCHO VCDs than MEGAN v2.1 (r = 0.32, p < 0.01). It suggests that the MEGAN v3.2 could simulate the spatial variations of BVOC emissions over the QTP better.

We further compared the spatial distributions of monthly mean HCHO VCDs simulated by experiments InBVOCv2.1 and InBVOCv3.2 against satellite observations (Fig. 3). Both experiments reproduced the spatial distribution of HCHO VCDs reasonably well (the spatial distribution of HCHO VCDs simulated with InBVOCv3.2 was almost identical to that with InBVOCv2.1 and is therefore not shown here), showing higher values over southeastern Tibet, northeastern Qinghai, and the Hengduan Mountains region, and relatively lower values over western QTP. The differences in simulated HCHO VCDs between InBVOCv2.1 and InBVOCv3.2 were most pronounced over southeastern Tibet and the Hengduan Mountains region, consistent with the spatial patterns of BVOC emissions (Fig. 2c, f). The spatial averaged HCHO VCDs from satellite observations, experiments InBVOCv2.1 and InBVOCv3.2 were 4.76 ± 2.26 , 3.32 ± 1.94 , and 2.91 ± 1.41 Pmolec cm⁻², respectively, suggesting that VOC emissions may be underestimated over the QTP. Li et al. (2023) reported that bottom-up VOC emissions from biogenic sources, anthropogenic sources (MEIC) and biomass burning (GFED 4.1) were 2.6, 1.1 and 8 times lower, respectively, than top-down estimates in Qinghai province.

A comparison across PFTs (Fig. S5) indicates that both experiments InBVOCv2.1 and InBVOCv3.2 performed better over grassland and cropland regions (Fig. S5h-j), with experiment InBVOCv3.2 showing higher correlation coefficients than experiment InBVOCv2.1. In contrast, simulated results over forested areas, with the exception of BETT, showed relatively lower accuracy. Although trees are the dominant emitters of BVOCs, the large diversity in species and emission strengths introduces

325

330





considerable uncertainties in the estimates. Nevertheless, experiment InBVOCv3.2 generally outperformed experiment InBVOCv2.1 across most forest types, whereas experiment InBVOCv2.1 performed better in shrubland regions.

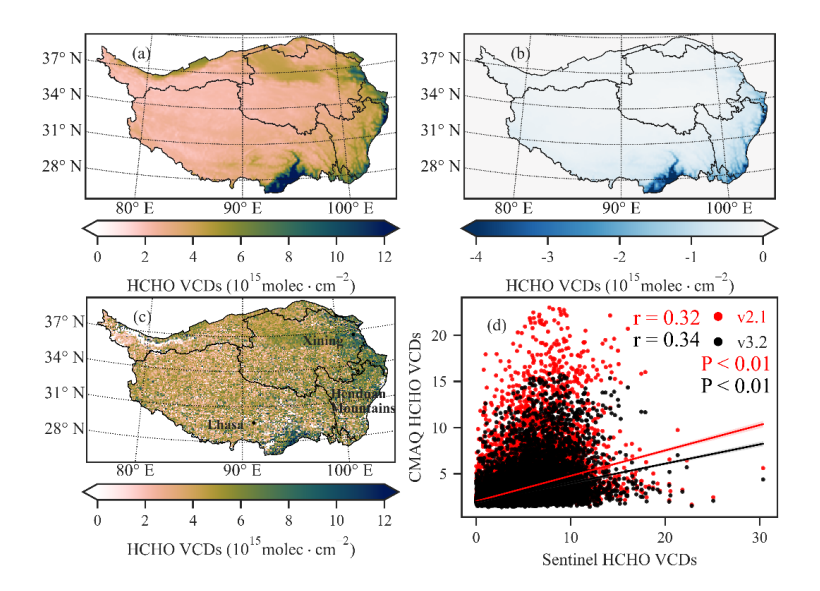


Figure 3: Spatial distribution of monthly mean HCHO vertical column densities (VCDs) (a) simulated by experiment InBVOCv2.1, (b) differences between InBVOCv3.2 and InBVOCv2.1, and (c) derived from Sentinel-5P observations. (d) Correlation between simulated and Sentinel-5P HCHO VCDs, with Pearson correlation coefficients (r) and p-values shown for experiments InBVOCv2.1 (red) and InBVOCv3.2 (black).

3.3.2 Constraints from Tropospheric Ozone Columns

Figure 4 presents the spatial distribution of monthly mean tropospheric column ozone (TCO) simulated by CMAQ with BVOC emissions from MEGAN v2.1 (experiment InBVOCv2.1) (the spatial distribution of TCO simulated with InBVOCv3.2 was almost identical to that with InBVOCv2.1 and is therefore not shown here), the differences in simulated TCO between InBVOCv3.2 and InBVOCv2.1, and the satellite-derived TCO. Similar to HCHO VCDs, both experiments (InBVOCv2.1 and InBVOCv3.2) reproduced the spatial distributions of TCO reasonably well, with higher values over the northwestern margin of the QTP, southeastern Tibet, northeastern Qinghai, and the Hengduan Mountains region, and lower values over the southwestern QTP. The simulated TCO differences between InBVOCv2.1 and InBVOCv3.2

335

340

345

350





were generally positive across most parts of the QTP, whereas negative values were observed over the eastern Hengduan Mountains region. The spatially averaged TCO from satellite observations, experiments InBVOCv2.1 and InBVOCv3.2 were 30.05 ± 3.71 , 42.69 ± 3.51 , and 42.95 ± 3.44 DU respectively. The correlation coefficients (r) between satellite-derived TCO and those simulated by the two experiments are similar (Fig. 4d).

A comparison across PFTs (Fig. S6) reveals that experiment InBVOCv3.2 achieves slightly better agreement with observations in grassland and cropland regions (Fig. S6h-j), though the improvement in correlations are marginal. In forest and shrubland regions, however, the differences between the two experiments (InBVOCv2.1 and InBVOCv3.2) become more complex: experiment InBVOCv3.2 shows slightly improved agreement with observations in deciduous areas but performs slightly worse in evergreen regions compared to experiment InBVOCv2.1. Ozone production is influenced not only by VOCs availability but also NO_x levels, with ozone production efficiency differing significantly between NO_x-limited and VOC-limited regimes (Zhao et al., 2009). Previous studies have demonstrated that BVOC emissions generally enhance O₃ concentrations under high-NO_x conditions, whereas under low-NO_x environments they may promote O₃ loss through increased consumption of O₃ by reaction with BVOC-derived peroxy radicals (Liaskoni et al., 2024; Rowlinson et al., 2020; Trainer et al., 1987; Williams et al., 2009; Zeng et al., 2008).

360

365





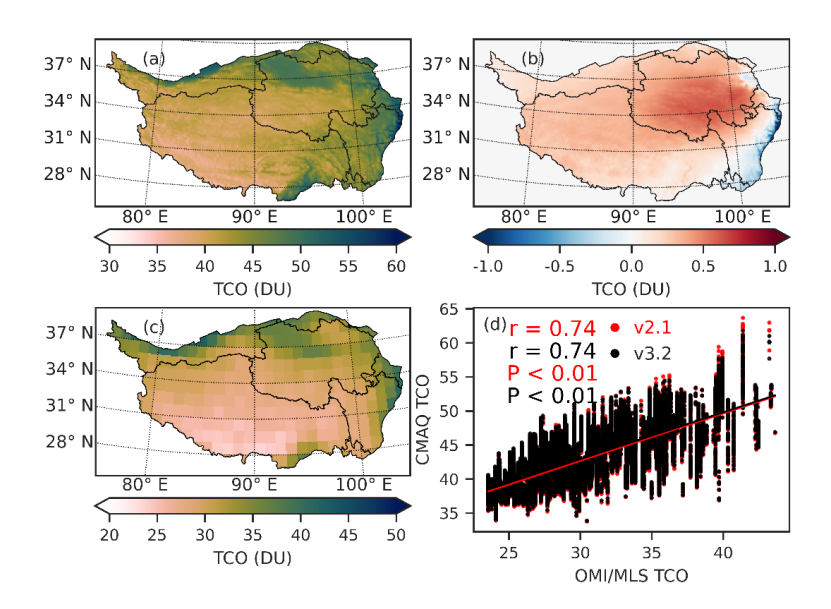


Figure 4: Spatial distribution of monthly mean tropospheric column ozone (TCO) (a) simulated by InBVOCv2.1, (b) differences between InBVOCv3.2 and InBVOCv2.1, and (c) derived from OMI/MLS observations. (d) Correlation between CMAQ-simulated and OMI/MLS derived TCO, with Pearson correlation coefficients (r) and p-values shown for experiments InBVOCv2.1 (red) and InBVOCv3.2 (black).

Overall, the performance differences between the two experiments are modest, although the simulated HCHO VCDs and TCO by experiment InBVOCv3.2 exhibit slightly better agreement with observations than those by experiment InBVOCv2.1. Previous studies have reported that MEGAN v2.1 tends to overestimate isoprene emissions (Carlton and Baker, 2011; Warneke et al., 2010; Emmerson et al., 2016). Ciccioli et al. (2023) further showed that a species-specific BVOCs model yields more accurate estimates of isoprene emissions compared to MEGAN v2.1. It should be noted, however, that satellite retrievals of both HCHO VCDs and TCO are subject to uncertainties, highlighting the need for direct BVOC concentration measurements to more robustly evaluate the performance of the two MEGAN versions over the QTP. In particular, in situ measurements of emission factors for locally prevalent trees and shrub species would help improve the accuracy of BVOC emission estimates in this region.

375

380

385





3.4 Impact of BVOC Emissions on Surface O₃ Formation

The CMAQ simulated monthly mean maximum daily 8 hour average (MDA8) O₃ concentration over the QTP for August 2022 were 122.51 (± 10.56) μg m⁻³, 125.38 (± 13.42) μg m⁻³, and 126.19 (± 11.42) μg m⁻³ for experiments NoBVOC, InBVOCv2.1 and InBVOCv3.2, respectively. The spatial distribution of MDA8 O₃ was generally consistent with observations across all experiments (Fig. 5a-c), with high values over northeastern Qinghai, the Hengduan Mountains region, and Lhasa, and relatively lower values over the southeastern Tibet. Although the InBVOCv2.1 simulation yields a slightly better correlation coefficient with observed MDA8 O₃ (Table 4), it simultaneously exhibits larger mean bias (MB) and root-mean-square error (RMSE) relative to InBVOCv3.2. These complementary metrics collectively demonstrate that WRF-CMAQ achieves overall better skill in reproducing surface O₃ when driven by BVOC emissions from MEGAN v3.2.

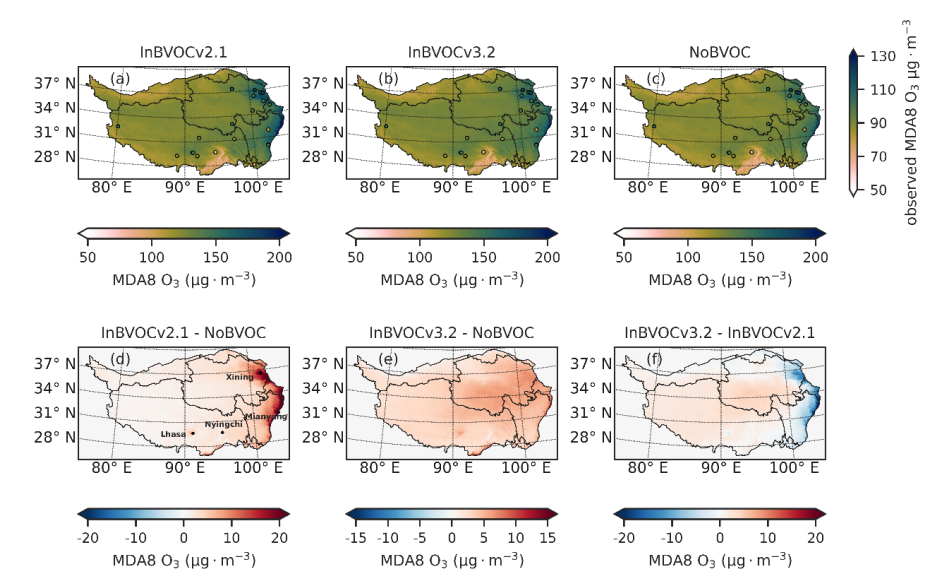


Figure 5: Spatial distribution of monthly mean maximum daily 8 hour average (MDA8) O_3 concentrations ($\mu g \ m^{-3}$) over the QTP in August 2022 from (a) InBVOCv2.1, (b) InBVOCv3.2, and (c) NoBVOC experiments. Differences in MDA8 O_3 between (d) InBVOCv2.1 and NoBVOC, (e) InBVOCv3.2 and NoBVOC, and (f) InBVOCv3.2 and InBVOCv2.1 experiments. Observation data from monitoring sites are overlaid as colored circles in panels (a) - (c).

Compared with the NoBVOC experiment, the experiments InBVOCv2.1 and InBVOCv3.2 substantially increased the monthly mean MDA8 O_3 concentration across the QTP, with an average increase of 2.87 \pm 3.72 μg m⁻³ (2.01% \pm 2.11%) and 3.68 \pm 1.40 μg m⁻³ (2.89% \pm 0.97%), respectively. Experiment

395

400

405

410





InBVOCv2.1 showed stronger increase in specific urban and topographically complex regions including Lhasa (8.84 μg m⁻³, 7.10%), Xining (19.12 μg m⁻³, 14.22%), and the Hengduan Mountains region (Fig. 5d). The maximum O₃ increase reached 53.03 μg m⁻³ (19.61%) in Mianyang, Sichuan, while the weakest effect occurred in Nyingchi (-1.59 μg m⁻³, -2.40%), Tibet. In contrast, experiment InBVOCv3.2 produced a more spatially uniform increase (Fig. 5e). Nevertheless, pronounced increase were still simulated in Lasha (5.89 μg m⁻³, 4.97%) and Xining (6.32 μg m⁻³, 5.13%), with a maximum increase of 15.59 μg m⁻³ (10.17%) in Mianyang and minimal effects near 0 μg m⁻³ in Nyingchi.

The differences in monthly mean MDA8 O₃ between the two experiments ranged from -37.50 μg m⁻³ to 4.96 μg m⁻³ (Fig. 5f). Most of the QTP (76.36% of grid cells) showed differences between 0 and 5 μg m⁻³. However, pronounced negative differences were observed in Lhasa and the eastern QTP, with the most substantial difference of -37.50 μg m⁻³ occurring in the Hengduan Mountains region. The pronounced differences in surface O₃ concentrations over Lhasa, Xining, and the Hengduan Mountains region correspond well to the large discrepancies in isoprene emissions between MEGAN2.1 and MEGAN3.2, highlighting the role of BVOCs in modeling regional ozone variability. However, in southeastern Tibet,

As an important O_3 precursor, isoprene strongly affects O_3 formation (Paulot et al., 2012), particularly under NO_x -rich environments such as urban areas (Liaskoni et al., 2024). For example, Li et al. (2007) reported that a 50% increase in isoprene emissions could enhance O_3 concentration by 10-50 μ g m⁻³ in urban Houston, USA. While under NO_x -limited environments they have limited impact. Jiang et al. (2019) showed that although isoprene emissions estimated by MEGAN v2.1 were about three times higher than those from a species-specific model (PSI) in Europe, the resulting increase in O_3 concentrations was limited to approximately 14 μ g mr⁻³ (~ 10%). They attributed this weak response to the relatively stronger sensitivity of O_3 formation to NO_x rather than VOCs, as well as the relatively low incremental in O_3 production compared to background O_3 levels in Europe. Ozone formation in most regions over the QTP is NO_x -limited, except in Lhasa, Xining and the Hengduan Mountains region (Fig. 6), where relatively high NO_x emissions make O_3 concentrations more responsive to VOCs variability (Ren et al., 2022; Zhang et al., 2022).

the difference in O₃ responses between experiments InBVOCv2.1 and InBVOCv3.2 remained small

despite substantial discrepancies in isoprene emissions.

420

425

430

435





One may notice the inconsistent spatial distribution between the BVOC emissions (Fig. 2) and the BVOC-induced variation in the MDA8 O_3 (Fig. 5). Specifically, at Xining, although the BVOC emission rate was relatively low (Fig. 2), the O_3 increase was very high (Fig. 5d). This is related to a transitional regime or VOC-limited regime in the area (Fig. 6c), where the BVOC emissions can interact with the anthropogenic NO_x emissions and increase O_3 . A similar situation occurred in Lasa. While in the southeastern Tibet, the increase of O_3 was not obvious (Fig. 5), though with a relatively higher BVOC emission rate (Fig. 2), which is due to the substantially low anthropogenic emissions and the NO_x -limited regime in the area.

The variation of BVOC emissions not only influence O₃ formation by acting as O₃ precursor but also change the O₃ formation regime (Lu et al., 2021; Wang et al., 2021b). Fig. 6c shows the spatial distribution of the O₃ formation regime for the NoBVOC experiment. The O₃ formation regime tended to be VOC-limited and transitional in urban areas, including Lhasa, northern Qinghai and the Hengduan Mountains region, whereas it was NO_x-limited in remote areas. In general, the area characterized by the NO_x-limited regime was 76.28%, and the corresponding values were 10.61% and 13.11% for the transitional and VOC-limited regimes. Compared with NoBVOC, the InBVOC experiment showed a shift from VOC-limited or transitional regimes to NO_x-limited regimes, especially in eastern QTP (Fig. 6a, b). Thus, the area with NO_x-limited regimes expanded by 6.76% and 3.33%, while the areas with transitional and VOC-limited regimes shrank by 5.19% and 2.76%, and 1.57% and 0.57%, respectively, in InBVOC2.1 and InBVOC3.2 experiments. This has implications for the design of future region-specific air quality management policies.

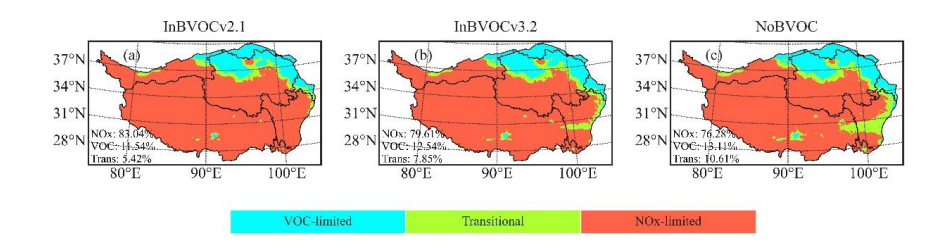


Figure 6: Spatial distributions of the O₃ formation regimes for experiments (a) InBVOC2.1, (b) InBVOC3.2 and (c) NoBVOC. Blue, green, and orange denote the VOC-limited, transitional, and NO_x-limited regimes, respectively. The total areas (%) with VOC-limited, transitional, and NO_x-limited regimes are shown in each subplot.





4 Conclusions

440

445

450

465

This study compared the differences in biogenic volatile organic compounds (BVOCs) emissions between MEGAN v2.1 and the latest MEGAN v3.2 over the Qinghai-Tibet Plateau (QTP), and their impact on surface MDA8 O₃ simulations for August 2022 by high-resolution WRF-CMAQ simulations. The results indicate notable differences between the two versions of MEGAN, with v3.2 giving a 44% less total BVOC emissions compared to v2.1. Isoprene emissions from MEGAN v3.2 is approximately 1.7 times lower, while monoterpene emissions are about 0.3 times higher than those from v2.1. Spatially, the differences are most pronounced in southeastern Tibet and the Hengduan Mountains, where dense forest and high biodiversity are present.

Despite these quantitative differences in BVOC emissions, WRF-CMAQ simulations using both MEGAN versions demonstrate relatively similar overall performance in capturing satellite-derived HCHO vertical column densities and tropospheric ozone columns, with simulations using v3.2 emissions exhibiting a modest improvement. The lack of in situ BVOC measurements limits a definitive assessment of the two MEGAN versions. Field campaigns targeting species-specific emission factors are needed to reduce uncertainties and constrain regional BVOC inventories.

WRF-CMAQ simulations with both inventories indicate increases in surface O₃ concentrations when BVOC emissions were incorporated, especially in regions with high NO_x emissions, such as Lhasa (4.97%-7.1% increase) and Xining (5.13%-14.22% increase). Across the QTP, the mean relative contribution of BVOCs to surface O₃ was 2-3%. However, substantial difference of -37.50 μg m⁻³ occurred along the eastern margin of the QTP, indicating sensitivity of ozone modelling in high-altitude cold regions to BVOC inventories.

Overall, the findings underscore the need to improve emission factors for local tree and shrub species and refine BVOCs emission estimates, particularly in high-NO_x regions, to achieve more reliable constrains on O_3 simulations over the QTP. Furthermore, the results highlight the critical role of NO_x emission control in mitigating O_3 formation in this ecologically sensitive region. This study provides new insights into the uncertainties associated with biogenic emission inventories and their implications for O_3 formation over the QTP. Future work should prioritize in situ BVOC emission for representative coniferous, broadleaf, and shrub communities on the QTP, updating local emission factor databases, and

https://doi.org/10.5194/egusphere-2025-5579 Preprint. Discussion started: 19 November 2025

© Author(s) 2025. CC BY 4.0 License.

470

475

480



EGUsphere Preprint repository

integrating NOx-VOC chemical mechanism observations. This will further reduce ozone prediction

errors and provide scientific basis for ecological conservation in the 'Third Pole'.

Code and data availability. The MAGEN code is freely available at https://bai.ess.uci.edu/megan. The

WRF model code is freely available at https://www.mmm.ucar.edu/models/wrf. The CMAQ and

SMOKE model code can be accessed at https://www.cmascenter.org/. The hourly surface ozone

concentrations used for model evaluation were obtained from the China National Environmental

Monitoring Center (https://air.cnemc.cn:18007/, last access: November 4, 2025). The surface

meteorological data used for model evaluation are available at National Climate Data Center (NCDC)

(https://www.ncei.noaa.gov/, last access: November 4, 2025). The MODIS MOD15A2H V6.1 and

MOD44B.006 data used for LAIv calculation and MODIS MCD12Q1.061 LC_Type5 used for PFTs

identification were obtained from the Google Earth Engine cloud platform. The global monthly

climatologies of surface air temperature and precipitation are from WorldClim

(https://www.worldclim.org/data/worldclim21.html, last access: November 4, 2025). The Sentinel-5P

TROPOMI daily offline level 3 (OFFL L3) HCHO dataset were obtained from the Google Earth Engine cloud platform. The OMI/MLS monthly-mean TCO dataset are available at https://acd-

ext.gsfc.nasa.gov/Data_services/cloud_slice/index.html#nd (last access: November 4, 2025). Data from

model simulations can be shared upon request via email to yyu@lzb.ac.cn.

Author contributions. PL carried out the simulations, processed the data, performed the analysis, and

drafted the manuscript. YY designed the study, performed the analysis, reviewed and finalized the

manuscript. SPZ reviewed and edited the manuscript. All the co-authors read and commented on the

490 manuscript.

Competing interests. The contact author has declared that none of the authors has any competing

interests.

495 **Financial support.** This study was supported by the Program of the State Key Laboratory of Cryospheric

Science and Frozen Soil Engineering, CAS (grant no. CSFSE-TZ-2411) and NSFC Excellent Young

Scientists Fund (grant no. 42422504).

21





References

- Appel, K. W., Bash, J. O., Fahey, K. M., Foley, K. M., Gilliam, R. C., Hogrefe, C., Hutzell, W. T., Kang, D., Mathur, R., Murphy, B. N., Napelenok, S. L., Nolte, C. G., Pleim, J. E., Pouliot, G. A., Pye, H. O. T., Ran, L., Roselle, S. J., Sarwar, G., Schwede, D. B., Sidi, F. I., Spero, T. L., and Wong, D. C.: The Community Multiscale Air Quality (CMAQ) model versions 5.3 and 5.3.1: system updates and evaluation, Geoscientific Model Development, 14, 2867–2897, https://doi.org/10.5194/gmd-14-2867-2021, 2021.
 - Atkinson, R. and Arey, J.: Gas-phase tropospheric chemistry of biogenic volatile organic compounds: a review, Atmospheric Environment, 37, 197–219, https://doi.org/10.1016/S1352-2310(03)00391-1, 2003.
 - Binkowski, F. S., Arunachalam, S., Adelman, Z., and Pinto, J. P.: Examining Photolysis Rates with a Prototype Online Photolysis Module in CMAQ, https://doi.org/10.1175/JAM2531.1, 2007.
- Bonan, G. B., Levis, S., Kergoat, L., and Oleson, K. W.: Landscapes as patches of plant functional types: An integrating concept for climate and ecosystem models, Global Biogeochemical Cycles, 16, 5-1-5–23, https://doi.org/10.1029/2000GB001360, 2002.
- Borge, R., Lumbreras, J., Pérez, J., de la Paz, D., Vedrenne, M., de Andrés, J. M., and Rodríguez, M. E.:

 Emission inventories and modeling requirements for the development of air quality plans. Application to

 Madrid (Spain), Science of The Total Environment, 466–467, 809–819,

 https://doi.org/10.1016/j.scitotenv.2013.07.093, 2014.
 - Bourtsoukidis, E., Bonn, B., Dittmann, A., Hakola, H., Hellén, H., and Jacobi, S.: Ozone stress as a driving force of sesquiterpene emissions: a suggested parameterisation, Biogeosciences, 9, 4337–4352, https://doi.org/10.5194/bg-9-4337-2012, 2012.
- Bourtsoukidis, E., Guenther, A., Wang, H., Economou, T., Lazoglou, G., Christodoulou, A., Christoudias, T., Nölscher, A., Yañez-Serrano, A. M., and Peñuelas, J.: Environmental Change Is Reshaping the Temperature Sensitivity of Sesquiterpene Emissions and Their Atmospheric Impacts, Global Change Biology, 31, e70258, https://doi.org/10.1111/gcb.70258, 2025.
- Che, M., Chen, B., Innes, J. L., Wang, G., Dou, X., Zhou, T., Zhang, H., Yan, J., Xu, G., and Zhao, H.:

 Spatial and temporal variations in the end date of the vegetation growing season throughout the Qinghai—
 Tibetan Plateau from 1982 to 2011, Agricultural and Forest Meteorology, 189–190, 81–90, https://doi.org/10.1016/j.agrformet.2014.01.004, 2014.
 - Chen, F. and Dudhia, J.: Coupling an Advanced Land Surface–Hydrology Model with the Penn State–NCAR MM5 Modeling System. Part I: Model Implementation and Sensitivity, 2001.
- Chen, F., Mitchell, K., Schaake, J., Xue, Y., Pan, H.-L., Koren, V., Duan, Q. Y., Ek, M., and Betts, A.: Modeling of land surface evaporation by four schemes and comparison with FIFE observations, Journal of Geophysical Research: Atmospheres, 101, 7251–7268, https://doi.org/10.1029/95JD02165, 1996.

565





Chen, J., Yan, F., and Lu, Q.: Spatiotemporal Variation of Vegetation on the Qinghai–Tibet Plateau and the Influence of Climatic Factors and Human Activities on Vegetation Trend (2000–2019), Remote Sensing, 12, 3150, https://doi.org/10.3390/rs12193150, 2020.

Chen, Y., Zhou, Y., NixiaCiren, Zhang, H., Wang, C., GesangDeji, and Wang, X.: Spatiotemporal variations of surface ozone and its influencing factors across Tibet: A Geodetector-based study, Science of The Total Environment, 813, 152651, https://doi.org/10.1016/j.scitotenv.2021.152651, 2022.

Ciccioli, P., Silibello, C., Finardi, S., Pepe, N., Ciccioli, P., Rapparini, F., Neri, L., Fares, S., Brilli, F.,
Mircea, M., Magliulo, E., and Baraldi, R.: The potential impact of biogenic volatile organic compounds
(BVOCs) from terrestrial vegetation on a Mediterranean area using two different emission models,
Agricultural and Forest Meteorology, 328, 109255, https://doi.org/10.1016/j.agrformet.2022.109255,
2023.

Collins, A. W., Rasch, A. P. J., Boville, A. B. A., McCaa, A. J., Williamson, A. D., Kiehl, A. J., Briegleb,
A. B. P., Bitz, A. C. M., Lin, A. S. J., Zhang, A. M., Dai, A. Y., and Division (CGD), C. U. C. F. A. R. (UCAR):National C. for A. R. (NCAR):NCAR E. S. L. (NESL):Climate and G. D.: Description of the NCAR Community Atmosphere Model (CAM 3.0), 2004.

DiMaria, C. A., Jones, D. B. A., Ferracci, V., Bloom, A. A., Worden, H. M., Seco, R., Vettikkat, L., Yáñez-Serrano, A. M., Guenther, A. B., Araujo, A., Goldstein, A. H., Langford, B., Cash, J., Harris, N. R. P.,
 Brown, L., Rinnan, R., Schobesberger, S., Holst, T., and Mak, J. E.: Optimizing the Temperature Sensitivity of the Isoprene Emission Model MEGAN in Different Ecosystems Using a Metropolis-Hastings Markov Chain Monte Carlo Method, Journal of Geophysical Research: Biogeosciences, 130, e2025JG008806, https://doi.org/10.1029/2025JG008806, 2025.

Emery, C., Jung, J., Koo, B., and Yarwood, G.: Improvements to CAMx snow cover treatments and Carbon Bond chemical mechanism for winter ozone, Final Report, 535, 2015.

Fares, S., Barta, C., Brilli, F., Centritto, M., Ederli, L., Ferranti, F., Pasqualini, S., Reale, L., Tricoli, D., and Loreto, F.: Impact of high ozone on isoprene emission, photosynthesis and histology of developing Populus alba leaves directly or indirectly exposed to the pollutant, Physiologia Plantarum, 128, 456–465, https://doi.org/10.1111/j.1399-3054.2006.00750.x, 2006.

Feldner, J., P. Ramacher, M. O., Karl, M., Quante, M., and L. Luttkus, M.: Analysis of the effect of abiotic stressors on BVOC emissions from urban green infrastructure in northern Germany, Environmental Science: Atmospheres, 2, 1132–1151, https://doi.org/10.1039/D2EA00038E, 2022.

Gao, Y., Ma, M., Yan, F., Su, H., Wang, S., Liao, H., Zhao, B., Wang, X., Sun, Y., Hopkins, J. R., Chen, Q., Fu, P., Lewis, A. C., Qiu, Q., Yao, X., and Gao, H.: Impacts of biogenic emissions from urban landscapes on summer ozone and secondary organic aerosol formation in megacities, Science of The Total Environment, 814, 152654, https://doi.org/10.1016/j.scitotenv.2021.152654, 2022.

Grote, R., Monson, R. K., and Niinemets, Ü.: Leaf-Level Models of Constitutive and Stress-Driven Volatile Organic Compound Emissions, in: Biology, Controls and Models of Tree Volatile Organic Compound Emissions, edited by: Niinemets, Ü. and Monson, R. K., Springer Netherlands, Dordrecht,

595

605





- 570 315–355, https://doi.org/10.1007/978-94-007-6606-8_12, 2013.
 - Gu, S., Guenther, A., and Faiola, C.: Effects of Anthropogenic and Biogenic Volatile Organic Compounds on Los Angeles Air Quality, Environ. Sci. Technol., 55, 12191–12201, https://doi.org/10.1021/acs.est.1c01481, 2021.
- Guenther, A., Karl, T., Harley, P., Wiedinmyer, C., Palmer, P. I., and Geron, C.: Estimates of global terrestrial isoprene emissions using MEGAN (Model of Emissions of Gases and Aerosols from Nature), Atmospheric Chemistry and Physics, 6, 3181–3210, 2006.
 - Guenther, A., Jiang, X., Shah, T., Huang, L., Kemball-Cook, S., and Yarwood, G.: Model of Emissions of Gases and Aerosol from Nature Version 3 (MEGAN3) for Estimating Biogenic Emissions, in: Air Pollution Modeling and its Application XXVI, Cham, 187–192, https://doi.org/10.1007/978-3-030-22055-6 29, 2020.
 - Guenther, A. B., Jiang, X., Heald, C. L., Sakulyanontvittaya, T., Duhl, T., Emmons, L. K., and Wang, X.: The Model of Emissions of Gases and Aerosols from Nature version 2.1 (MEGAN2.1): an extended and updated framework for modeling biogenic emissions, Geoscientific Model Development, 5, 1471–1492, https://doi.org/10.5194/gmd-5-1471-2012, 2012.
- Guion, A., Turquety, S., Cholakian, A., Polcher, J., Ehret, A., and Lathière, J.: Biogenic isoprene emissions, dry deposition velocity, and surface ozone concentration during summer droughts, heatwaves, and normal conditions in southwestern Europe, Atmospheric Chemistry and Physics, 23, 1043–1071, https://doi.org/10.5194/acp-23-1043-2023, 2023.
- Guo, H., Zhang, Y., Ran, H., Zeng, J., and Wang, X.: Improving Light-Dependent Monoterpene Emission

 Parameterizations to Enhance Chemical Transport Model Predictions of Ozone and SOA in South China,

 Journal of Geophysical Research: Atmospheres, 130, e2025JD044435,

 https://doi.org/10.1029/2025JD044435, 2025.
 - Han, H., Yin, Y., Zhao, Y., and Qin, F.: Spatiotemporal Variations in Fractional Vegetation Cover and Their Responses to Climatic Changes on the Qinghai–Tibet Plateau, Remote Sensing, 15, 2662, https://doi.org/10.3390/rs15102662, 2023.
 - Hong, S.-Y. and Lim, J.: The WRF Single-Moment 6-Class Microphysics Scheme (WSM6), Asia-pacific Journal of Atmospheric Sciences, 2006.
 - Hong, S.-Y., Noh, Y., and Dudhia, J.: A New Vertical Diffusion Package with an Explicit Treatment of Entrainment Processes, https://doi.org/10.1175/MWR3199.1, 2006.
- Hu, Y., Yu, H., Kang, S., Yang, J., Chen, X., Yin, X., and Chen, P.: Modeling the transport of PM10, PM2.5, and O3 from South Asia to the Tibetan Plateau, Atmospheric Research, 303, 107323, https://doi.org/10.1016/j.atmosres.2024.107323, 2024.
 - Huang, L., Zhao, X., Chen, C., Tan, J., Li, Y., Chen, H., Wang, Y., Li, L., Guenther, A., and Huang, H.: Uncertainties of biogenic VOC emissions caused by land cover data and implications on ozone mitigation strategies for the Yangtze river Delta region, Atmospheric Environment, 337, 120765,





- https://doi.org/10.1016/j.atmosenv.2024.120765, 2024.
- Huang, T., Liu, M., Xing, R., Men, Y., and Shen, G.: Threat of air pollution in the cleanest plateau, Innovation (Camb), 4, 100390, https://doi.org/10.1016/j.xinn.2023.100390, 2023.
- Jiang, J., Aksoyoglu, S., Ciarelli, G., Oikonomakis, E., El-Haddad, I., Canonaco, F., O'Dowd, C.,
 Ovadnevaite, J., Minguillón, M. C., Baltensperger, U., and Prévôt, A. S. H.: Effects of two different biogenic emission models on modelled ozone and aerosol concentrations in Europe, Atmospheric Chemistry and Physics, 19, 3747–3768, https://doi.org/10.5194/acp-19-3747-2019, 2019.
- Jin, X. and Holloway, T.: Spatial and temporal variability of ozone sensitivity over China observed from the Ozone Monitoring Instrument, Journal of Geophysical Research: Atmospheres, 120, 7229–7246,
 https://doi.org/10.1002/2015JD023250, 2015.
 - Kain, J. S.: The Kain-Fritsch Convective Parameterization: An Update, 2004.
 - Klinger, L. F., Li, Q.-J., Guenther, A. B., Greenberg, J. P., Baker, B., and Bai, J.-H.: Assessment of volatile organic compound emissions from ecosystems of China, Journal of Geophysical Research: Atmospheres, 107, ACH 16-1-ACH 16-21, https://doi.org/10.1029/2001JD001076, 2002.
- Kuang, X. and Jiao, J. J.: Review on climate change on the Tibetan Plateau during the last half century, Journal of Geophysical Research: Atmospheres, 121, 3979–4007, https://doi.org/10.1002/2015JD024728, 2016.
- Li, G., Zhang, R., Fan, J., and Tie, X.: Impacts of biogenic emissions on photochemical ozone production in Houston, Texas, Journal of Geophysical Research: Atmospheres, 112, https://doi.org/10.1029/2006JD007924, 2007.
 - Li, L., Cao, J., and Hao, Y.: Spatial and species-specific responses of biogenic volatile organic compound (BVOC) emissions to elevated ozone from 2014–2020 in China, Science of The Total Environment, 868, 161636, https://doi.org/10.1016/j.scitotenv.2023.161636, 2023a.
- Li, S., Zhang, H., Zhou, X., Yu, H., and Li, W.: Enhancing protected areas for biodiversity and ecosystem services in the Qinghai–Tibet Plateau, Ecosystem Services, 43, 101090, https://doi.org/10.1016/j.ecoser.2020.101090, 2020.
 - Li, W., Han, X., Li, J., Lun, X., and Zhang, M.: Assessment of surface ozone production in Qinghai, China with satellite-constrained VOCs and NOx emissions, Science of The Total Environment, 905, 166602, https://doi.org/10.1016/j.scitotenv.2023.166602, 2023b.
- 635 Li, X., Qin, M., Li, L., Gong, K., Shen, H., Li, J., and Hu, J.: Examining the implications of photochemical indicators for O₃–NO_x–VOC sensitivity and control strategies: a case study in the Yangtze River Delta (YRD), China, Atmospheric Chemistry and Physics, 22, 14799–14811, https://doi.org/10.5194/acp-22-14799-2022, 2022.
- Liaskoni, M., Huszár, P., Bartík, L., Prieto Perez, A. P., Karlický, J., and Šindelářová, K.: The long-term impact of biogenic volatile organic compound emissions on urban ozone patterns over central Europe:

655

665





contributions from urban and rural vegetation, Atmospheric Chemistry and Physics, 24, 13541–13569, https://doi.org/10.5194/acp-24-13541-2024, 2024.

López-Pujol, J., Zhang, F.-M., and Ge, S.: Plant Biodiversity in China: Richly Varied, Endangered, and in Need of Conservation, Biodivers Conserv, 15, 3983–4026, https://doi.org/10.1007/s10531-005-3015-2, 2006.

Loreto, F. and Schnitzler, J.-P.: Abiotic stresses and induced BVOCs, Trends in Plant Science, 15, 154–166, https://doi.org/10.1016/j.tplants.2009.12.006, 2010.

Lou, C., Jiang, F., Tian, X., Zou, Q., Zheng, Y., Shen, Y., Feng, S., Chen, J., Zhang, L., Jia, M., and Xu,
J.: Modeling the biogenic isoprene emission and its impact on ozone pollution in Zhejiang province,
China, Science of The Total Environment, 865, 161212, https://doi.org/10.1016/j.scitotenv.2022.161212,
2023

Lu, X., Ye, X., Zhou, M., Zhao, Y., Weng, H., Kong, H., Li, K., Gao, M., Zheng, B., Lin, J., Zhou, F., Zhang, Q., Wu, D., Zhang, L., and Zhang, Y.: The underappreciated role of agricultural soil nitrogen oxide emissions in ozone pollution regulation in North China, Nat Commun, 12, 5021, https://doi.org/10.1038/s41467-021-25147-9, 2021.

Lu, X., Cao, L., Ding, H., Gao, M., and Meng, X.: The relationship between the altitude and the simulations of ozone and NO2 by WRF-Chem for the Tibetan Plateau, Atmospheric Environment, 274, 118981, https://doi.org/10.1016/j.atmosenv.2022.118981, 2022.

Lun, X., Lin, Y., Chai, F., Fan, C., Li, H., and Liu, J.: Reviews of emission of biogenic volatile organic compounds (BVOCs) in Asia, Journal of Environmental Sciences, 95, 266–277, https://doi.org/10.1016/j.jes.2020.04.043, 2020.

Ma, M., Gao, Y., Wang, Y., Zhang, S., Leung, L. R., Liu, C., Wang, S., Zhao, B., Chang, X., Su, H., Zhang, T., Sheng, L., Yao, X., and Gao, H.: Substantial ozone enhancement over the North China Plain from increased biogenic emissions due to heat waves and land cover in summer 2017, Atmospheric Chemistry and Physics, 19, 12195–12207, https://doi.org/10.5194/acp-19-12195-2019, 2019.

Nagalingam, S., Wang, H., Kim, S., and Guenther, A.: Unexpectedly strong heat stress induction of monoterpene, methylbutenol, and other volatile emissions for conifers in the cypress family (Cupressaceae), Science of The Total Environment, 956, 177336, https://doi.org/10.1016/j.scitotenv.2024.177336, 2024.

Olson, D. M., Dinerstein, E., Wikramanayake, E. D., Burgess, N. D., Powell, G. V. N., Underwood, E. C., D'amico, J. A., Itoua, I., Strand, H. E., Morrison, J. C., Loucks, C. J., Allnutt, T. F., Ricketts, T. H., Kura, Y., Lamoreux, J. F., Wettengel, W. W., Hedao, P., and Kassem, K. R.: Terrestrial Ecoregions of the World: A New Map of Life on Earth: A new global map of terrestrial ecoregions provides an innovative tool for conserving biodiversity, BioScience, 51, 933–938, https://doi.org/10.1641/0006-3568(2001)051%255B0933:TEOTWA%255D2.0.CO;2, 2001.

Paulot, F., Henze, D. K., and Wennberg, P. O.: Impact of the isoprene photochemical cascade on tropical ozone, Atmospheric Chemistry and Physics, 12, 1307–1325, https://doi.org/10.5194/acp-12-1307-2012,





2012.

680

685

695

705

710

Peron, A., Kaser, L., Fitzky, A. C., Graus, M., Halbwirth, H., Greiner, J., Wohlfahrt, G., Rewald, B., Sandén, H., and Karl, T.: Combined effects of ozone and drought stress on the emission of biogenic volatile organic compounds from *Quercus robur* L., Biogeosciences, 18, 535–556, https://doi.org/10.5194/bg-18-535-2021, 2021.

Pichersky, E. and Gershenzon, J.: The formation and function of plant volatiles: perfumes for pollinator attraction and defense, Current Opinion in Plant Biology, 5, 237–243, https://doi.org/10.1016/S1369-5266(02)00251-0, 2002.

Possell, M. and Loreto, F.: The Role of Volatile Organic Compounds in Plant Resistance to Abiotic Stresses: Responses and Mechanisms, in: Biology, Controls and Models of Tree Volatile Organic Compound Emissions, edited by: Niinemets, Ü. and Monson, R. K., Springer Netherlands, Dordrecht, 209–235, https://doi.org/10.1007/978-94-007-6606-8 8, 2013.

Ren, J., Guo, F., and Xie, S.: Diagnosing ozone–NO_x–VOC sensitivity and revealing causes of ozone increases in China based on 2013–2021 satellite retrievals, Atmospheric Chemistry and Physics, 22, 15035–15047, https://doi.org/10.5194/acp-22-15035-2022, 2022.

Rowlinson, M. J., Rap, A., Hamilton, D. S., Pope, R. J., Hantson, S., Arnold, S. R., Kaplan, J. O., Arneth, A., Chipperfield, M. P., Forster, P. M., and Nieradzik, L.: Tropospheric ozone radiative forcing uncertainty due to pre-industrial fire and biogenic emissions, Atmospheric Chemistry and Physics, 20, 10937–10951, https://doi.org/10.5194/acp-20-10937-2020, 2020.

Seco, R., Holst, T., Davie-Martin, C. L., Simin, T., Guenther, A., Pirk, N., Rinne, J., and Rinnan, R.: Strong isoprene emission response to temperature in tundra vegetation, Proceedings of the National Academy of Sciences, 119, e2118014119, https://doi.org/10.1073/pnas.2118014119, 2022.

700 Sillman, S. and He, D.: Some theoretical results concerning O3-NOx-VOC chemistry and NOx-VOC indicators, Journal of Geophysical Research: Atmospheres, 107, ACH 26-1-ACH 26-15, https://doi.org/10.1029/2001JD001123, 2002.

Šimpraga, M., Ghimire, R. P., Van Der Straeten, D., Blande, J. D., Kasurinen, A., Sorvari, J., Holopainen, T., Adriaenssens, S., Holopainen, J. K., and Kivimäenpää, M.: Unravelling the functions of biogenic volatiles in boreal and temperate forest ecosystems, Eur J Forest Res, 138, 763–787, https://doi.org/10.1007/s10342-019-01213-2, 2019.

Su, Y., Guo, Q., Hu, T., Guan, H., Jin, S., An, S., Chen, X., Guo, K., Hao, Z., Hu, Y., Huang, Y., Jiang, M., Li, J., Li, Z., Li, X., Li, X., Liang, C., Liu, R., Liu, Q., Ni, H., Peng, S., Shen, Z., Tang, Z., Tian, X., Wang, X., Wang, R., Xie, Z., Xie, Y., Xu, X., Yang, X., Yang, Y., Yu, L., Yue, M., Zhang, F., and Ma, K.: An updated Vegetation Map of China (1:1000000), Science Bulletin, 65, 1125–1136, https://doi.org/10.1016/j.scib.2020.04.004, 2020.

Sun, Q., Li, B., Zhou, G., Jiang, Y., and Yuan, Y.: Delayed autumn leaf senescence date prolongs the growing season length of herbaceous plants on the Qinghai–Tibetan Plateau, Agricultural and Forest Meteorology, 284, 107896, https://doi.org/10.1016/j.agrformet.2019.107896, 2020.





- Trainer, M., Williams, E. J., Parrish, D. D., Buhr, M. P., Allwine, E. J., Westberg, H. H., Fehsenfeld, F. C., and Liu, S. C.: Models and observations of the impact of natural hydrocarbons on rural ozone, Nature, 329, 705–707, https://doi.org/10.1038/329705a0, 1987.
- Trimmel, H., Hamer, P., Mayer, M., Schreier, S. F., Weihs, P., Eitzinger, J., Sandén, H., Fitzky, A. C.,
 Richter, A., Calvet, J.-C., Bonan, B., Meurey, C., Vallejo, I., Eckhardt, S., Santos, G. S., Oumami, S.,
 Arteta, J., Marécal, V., Tarrasón, L., Karl, T., and Rieder, H. E.: The influence of vegetation drought stress on formaldehyde and ozone distributions over a central European city, Atmospheric Environment, 304, 119768, https://doi.org/10.1016/j.atmosenv.2023.119768, 2023.
- Wang, H., Wu, Q., Liu, H., Wang, Y., Cheng, H., Wang, R., Wang, L., Xiao, H., and Yang, X.: Sensitivity of biogenic volatile organic compound emissions to leaf area index and land cover in Beijing,
 Atmospheric Chemistry and Physics, 18, 9583–9596, https://doi.org/10.5194/acp-18-9583-2018, 2018.
 - Wang, H., Wu, K., Liu, Y., Sheng, B., Lu, X., He, Y., Xie, J., Wang, H., and Fan, S.: Role of Heat Wave-Induced Biogenic VOC Enhancements in Persistent Ozone Episodes Formation in Pearl River Delta, Journal of Geophysical Research: Atmospheres, 126, e2020JD034317, https://doi.org/10.1029/2020JD034317, 2021a.
- Wang, H., Lu, X., Seco, R., Stavrakou, T., Karl, T., Jiang, X., Gu, L., and Guenther, A. B.: Modeling Isoprene Emission Response to Drought and Heatwaves Within MEGAN Using Evapotranspiration Data and by Coupling With the Community Land Model, Journal of Advances in Modeling Earth Systems, 14, e2022MS003174, https://doi.org/10.1029/2022MS003174, 2022.
- Wang, H., Welch, A., Nagalingam, S., Leong, C., Kittitananuvong, P., Barsanti, K. C., Sheesley, R. J.,
 735 Czimczik, C. I., and Guenther, A. B.: Arctic Heatwaves Could Significantly Influence the Isoprene
 Emissions From Shrubs, Geophysical Research Letters, 51, e2023GL107599,
 https://doi.org/10.1029/2023GL107599, 2024a.
- Wang, H., Qiu, J., Liu, Y., Fan, Q., Lu, X., Zhang, Y., Wu, K., Shen, A., Xu, Y., Jin, Y., Zhu, Y., Sun, J., and Wang, H.: MEIAT-CMAQ: A modular emission inventory allocation tool for Community Multiscale
 740 Air Quality Model, Atmospheric Environment, 331, 120604, https://doi.org/10.1016/j.atmosenv.2024.120604, 2024b.
 - Wang, L., Lun, X., Wu, J., Wang, Q., Tao, J., Dou, X., and Zhang, Z.: Investigation of biogenic volatile organic compounds emissions in the Qinghai-Tibetan Plateau, Science of The Total Environment, 902, 165877, https://doi.org/10.1016/j.scitotenv.2023.165877, 2023a.
- Wang, P., Zhang, Y., Gong, H., Zhang, H., Guenther, A., Zeng, J., Wang, T., and Wang, X.: Updating Biogenic Volatile Organic Compound (BVOC) Emissions With Locally Measured Emission Factors in South China and the Effect on Modeled Ozone and Secondary Organic Aerosol Production, Journal of Geophysical Research: Atmospheres, 128, e2023JD039928, https://doi.org/10.1029/2023JD039928, 2023b.
- Wang, W., van der A, R., Ding, J., van Weele, M., and Cheng, T.: Spatial and temporal changes of the ozone sensitivity in China based on satellite and ground-based observations, Atmospheric Chemistry and





- Physics, 21, 7253-7269, https://doi.org/10.5194/acp-21-7253-2021, 2021b.
- Wiedinmyer, C., Kimura, Y., McDonald-Buller, E. C., Emmons, L. K., Buchholz, R. R., Tang, W., Seto,
 K., Joseph, M. B., Barsanti, K. C., Carlton, A. G., and Yokelson, R.: The Fire Inventory from NCAR
 version 2.5: an updated global fire emissions model for climate and chemistry applications, Geoscientific
 Model Development, 16, 3873–3891, https://doi.org/10.5194/gmd-16-3873-2023, 2023.
 - Williams, J. E., Scheele, M. P., van Velthoven, P. F. J., Cammas, J.-P., Thouret, V., Galy-Lacaux, C., and Volz-Thomas, A.: The influence of biogenic emissions from Africa on tropical tropospheric ozone during 2006: a global modeling study, Atmospheric Chemistry and Physics, 9, 5729–5749, https://doi.org/10.5194/acp-9-5729-2009, 2009.
 - Xu, C., Lin, J., Kong, H., Jin, J., Chen, L., and Xu, X.: Rapid Increases of Ozone Concentrations over Tibetan Plateau Caused by Local and Non-Local Factors, EGUsphere, 1–22, https://doi.org/10.5194/egusphere-2024-3471, 2024.
- Yang, J., Kang, S., Ji, Z., Chen, X., Yang, S., Lee, S.-Y., de Foy, B., and Chen, D.: A hybrid method for PM2.5 source apportionment through WRF-Chem simulations and an assessment of emission-reduction measures in western China, Atmospheric Research, 236, 104787, https://doi.org/10.1016/j.atmosres.2019.104787, 2020.
- Ye, X., Zhang, L., Wang, X., Lu, X., Jiang, Z., Lu, N., Li, D., and Xu, J.: Spatial and temporal variations of surface background ozone in China analyzed with the grid-stretching capability of GEOS-Chem High Performance, Science of The Total Environment, 914, 169909, https://doi.org/10.1016/j.scitotenv.2024.169909, 2024.
 - Yin, L., Xu, Z., Liu, M., Xu, T., Wang, T., Liao, W., Li, M., Cai, X., Kang, L., Zhang, H., and Song, Y.: Estimation of biogenic volatile organic compound (BVOC) emissions in China using WRF-CLM-MEGAN coupled model, Biogeosciences Discussions, 1–30, https://doi.org/10.5194/bg-2019-458, 2020.
- Yin, X., Rupakheti, D., Zhang, G., Luo, J., Kang, S., de Foy, B., Yang, J., Ji, Z., Cong, Z., Rupakheti, M., Li, P., Hu, Y., and Zhang, Q.: Surface ozone over the Tibetan Plateau controlled by stratospheric intrusion, Atmospheric Chemistry and Physics, 23, 10137–10143, https://doi.org/10.5194/acp-23-10137-2023, 2023.
- You, Q., Fraedrich, K., Ren, G., Pepin, N., and Kang, S.: Variability of temperature in the Tibetan Plateau based on homogenized surface stations and reanalysis data, International Journal of Climatology, 33, 1337–1347, https://doi.org/10.1002/joc.3512, 2013.
 - Yu, H., Holopainen, J. K., Kivimäenpää, M., Virtanen, A., and Blande, J. D.: Potential of Climate Change and Herbivory to Affect the Release and Atmospheric Reactions of BVOCs from Boreal and Subarctic Forests, Molecules, 26, 2283, https://doi.org/10.3390/molecules26082283, 2021.
- Yu, J., Han, K. M., Song, C. H., Lee, K., Lee, S., Kim, Y., Woo, J.-H., Kim, S., and Wisthaler, A.: Evaluation of biogenic emissions from three different vegetation distributions in South Korea, Atmospheric Environment, 296, 119588, https://doi.org/10.1016/j.atmosenv.2023.119588, 2023.





Zeng, G., Pyle, J. A., and Young, P. J.: Impact of climate change on tropospheric ozone and its global budgets, Atmospheric Chemistry and Physics, 8, 369–387, https://doi.org/10.5194/acp-8-369-2008, 2008.

Zhang, D.-C., Ye, J.-X., and Sun, H.: Quantitative approaches to identify floristic units and centres of species endemism in the Qinghai-Tibetan Plateau, south-western China, Journal of Biogeography, 43, 2465–2476, https://doi.org/10.1111/jbi.12819, 2016.

Zhang, S., Lyu, Y., Yang, X., Yuan, L., Wang, Y., Wang, L., Liang, Y., Qiao, Y., and Wang, S.: Modeling Biogenic Volatile Organic Compounds Emissions and Subsequent Impacts on Ozone Air Quality in the Sichuan Basin, Southwestern China, Front. Ecol. Evol., 10, https://doi.org/10.3389/fevo.2022.924944, 2022.

Zhao, C., Wang, Y., and Zeng, T.: East China Plains: A "Basin" of Ozone Pollution, Environ. Sci. Technol., 43, 1911–1915, https://doi.org/10.1021/es8027764, 2009.

Zhu, L., Mickley, L. J., Jacob, D. J., Marais, E. A., Sheng, J., Hu, L., Abad, G. G., and Chance, K.: Longterm (2005–2014) trends in formaldehyde (HCHO) columns across North America as seen by the OMI satellite instrument: Evidence of changing emissions of volatile organic compounds, Geophysical Research Letters, 44, 7079–7086, https://doi.org/10.1002/2017GL073859, 2017.

Ziemke, J. R., Chandra, S., Duncan, B. N., Froidevaux, L., Bhartia, P. K., Levelt, P. F., and Waters, J. W.: Tropospheric ozone determined from Aura OMI and MLS: Evaluation of measurements and comparison with the Global Modeling Initiative's Chemical Transport Model, Journal of Geophysical Research: Atmospheres, 111, https://doi.org/10.1029/2006JD007089, 2006.

Ziemke, J. R., Chandra, S., Labow, G. J., Bhartia, P. K., Froidevaux, L., and Witte, J. C.: A global climatology of tropospheric and stratospheric ozone derived from Aura OMI and MLS measurements, Atmospheric Chemistry and Physics, 11, 9237–9251, https://doi.org/10.5194/acp-11-9237-2011, 2011.

810

795

800

805